Mineralogy and Petrology (1989) 40: 207–224

Mineralogy and Petrology

The Petrography and Composition of Phlogopite Micas from the Blue Ball Kimberlite, Arkansas: a Record of Chemical Evolution During Crystallization

C. R. Neal and L. A. Taylor

Department of Geological Sciences, University of Tennessee, Knoxville, Tennessee, U.S.A.

With 8 Figures

Received November 7, 1988;
accepted February 28, 1989

Summary

The Blue Ball kimberlite, Scott County, Arkansas, contains between 23 and 36 modal % phlogopite. Phlogopite is present as phenocrysts, a groundmass phase, and as coronas around serpentinized olivine phenocrysts. Intermediate and reverse pleochroism, seen in phenocryst cores and the majority of groundmass phlogopites, can be correlated with the mineral chemistry. Reverse pleochroism, exhibited by phenocryst rims, rare groundmass grains, and phlogopites forming coronas around olivine, is generally accompanied by an increase in total Fe (as FeO) and a decrease in Al_2O_3. Analyses of those phlogopites whoch exhibit reverse pleochroism have high cation totals, indicative of the presence of Fe^{3+}. We suggest that these pleochroic schemes are a function of Fe^{3+} in the tetrahedral site, which is expressed in terms of $\Delta T = [8 - (Si + Al)]$. All Blue Ball phlogopites have positive values for ΔT, but reverse pleochroism is found only when $\Delta T > 0.6$, indicative of increased Fe^{3+} in the residual magma. It is concluded that phlogopite was on the liquidus throughout practically all of the kimberlite crystallization, because of the wide range in phlogopite compositions and the general decrease in Ba from micas exhibiting intermediate to reverse pleochroism. Variations of MG#, Ti, Ba, Si, and Al within the phlogopites have been used to trace the crystallization of other phases present in the kimberlite, namely olivine and spinel (chromite and titanomagnetite). Olivine was an early crystallizing phase, causing a decrease in MG# and Si, and an increase in Ti and Al in the phlogopites, a reflection of residual magma composition. Minor chromite also crystallized at this time, but was not of sufficient quantity to override the effect of olivine fractionation on the residual magma. Widespread Titano-magnetite crystallization occurred as olivine fractionation ceased, causing an increase in MG# and Si, and a decrease in Ti and Al. By examining these chemical variations with ΔT, the evolution of the Blue Ball kimberlite has been determined.

Zusammenfassung

Petrographie und Zusammensetzung phlogopitischer Glimmer aus dem Blue Ball Kimberlit, Arkansas: chemische Evolution während der Kristallisation

Der Blue Ball Kimberlit, Scott County, Arkansas, enthält zwischen 23 und 36% Phlogopit (modal). Dieser kommt in idiomorphen Kristallen, als Grundmasse, und als Coronas um serpentinisierte Olivinkristalle vor. Verschiedene Arten von Pleochroismus, die man in den Kernen von Kristallen und in der Mehrzahl der Phlogopite in der Grundmasse erkennen kann, lassen sich mit der Mineralchemie korrelieren. Reverser Pleochroismus ist an den Rändern von Kristallen, selten in Grundkörnern der Grundmasse, und in Phlogopiten die Coronas in Olivin bilden, zu beobachten. Diese Erscheinung wird im allgemeinen von einer Zunahme des Gesamt-Eisens (als FeO) und einer Abnahme der Al_2O_3-Gehalte begleitet. Analysen jener Phlogopite, die reversen Pleochroismus zeigen, haben hohe Gesamtwerte an Kationen und dies weist auf die Anwesenheit von Fe^{3+} hin. Wir interpretieren diesen Pleochroismus als eine Funktion des Fe^{3+} in der Tetraeder-Position, die sich als $\Delta T = 8 - (Si + Al)$ ausdrücken läßt. Alle Phlogopite von Blue Ball haben positive Werte für ΔT, aber reverser Pleochroismus tritt nur dort auf, wo $\Delta T > 0.6$, was widerum auf eine Zunahme von Fe^{3+} im residualen Magma hinweist. Phlogopit war praktisch während der gesamten Kristallisation des Kimberlits am Liquidus, und diese Annahme wird auch durch das weite Feld der Phlogopit-Zusammensetzungen und durch die allgemeine Abahme der Ba-Gehalte in Glimmern mit intermediärem bis reversem Pleochroismus unterstützt. Variationen von MG#, Ti, Ba, Si und Al in den Phlogopiten wurden benutzt, um die Kristallisation von Olivin und Spinellen (Chromit und Titanomagnetit) zu verfolgen. Olivin hat früh kristallisiert und führte zu einer Abnahme von MG# und Si und einer Zunahme von Ti und Al in den Phlogopiten. Auch kleinere Mengen von Chromit kristallisierten zu dieser Zeit, dies war jedoch nicht ausreichend, um den Effekt der Olivin-Fraktionierung auf die Restschmelze aufzuheben. Titanomagnetit-Kristallisation setzte mit aufhörender Olivinfraktionierung ein und führte zu einer Zunahme von Mg und Si und einer Abnahme von Ti und Al. Eine Überprüfung der chemischen Variationen und Vergleich mit ΔT Werten tragen wesentlich zur Kenntnis der Evolution des Blue Ball Kimberlites bei.

Introduction

The occurrence of phlogopite mica in mantle-derived materials demonstrates the presence of water in the Earth's interior. Hydrous minerals within the mantle will have a profound affect on the melting point of peridotite, and also on the composition of the resultant melt (e.g., *Kushiro*, 1975; *Wyllie*, 1978). The stability of mica within a mantle regime has been examined by *Eggler* and *Wendlandt* (1978), *Wyllie* (1979), and *Wendlandt* and *Eggler* (1980). These authors concluded that phlogopite may be stable down to 150–200 km and temperatures in excess of 1200 °C. However, this is dependent upon the CO_2/H_2O ratio of the fluid phase in the system. The greater this ratio, the greater the stability of phlogopite (*Wyllie*, 1979).

Most commonly, mantle phlogopite is brought to the surface in kimberlites, where it has two major parageneses: 1) within mantle peridotite xenoliths, and 2) as single crystals within the kimberlite matrix (megacrysts, xenocrysts, phenocrysts, and groundmass). Peridotite xenoliths containing phlogopite have received a disproportionate amount of attention because of their links with mantle metasomatism (see *Delaney* et al., 1980; *Lloyd* and *D. Bailey*, 1975; Boettcher et al., 1979; Wass and Rogers, 1980; *D. Bailey*, 1982, 1984; *Menzies* and *Hawkesworth*, 1987, and papers

therein). A variety of phlogopite-bearing xenoliths have been classified on the basis of their constituent minerals (e.g., *Erlank* et al., 1982; *Dawson* and *Smith*, 1977; *Jones*, 1984).

Although much work has been conducted on xenolith micas, until recently little has been reported on the phenocryst/groundmass phlogopites in kimberlite matrices. Studies that have concentrated on kimberlite rather than xenolithic micas have highlighted the significance of **tetraferriphlogopites** (i.e., phlogopites containing tetrahedral Fe^{3+}), in the kimberlite groundmass. These phlogopites are reported to exhibit *reverse pleochroism* (*Dawson* and *Smith*, 1975; *Smith* et al., 1978; *Mitchell* and *Meyer*, 1980; *Farmer* and *Boettcher*, 1981; *Scott*, 1981; *Boctor* and *Boyd*, 1982; *Hunter* et al., 1984).

In this paper, we present the results of a study on the abundant phlogopite present in the Blue Ball kimberlite, Scott County, Arkansas. As an outgrowth of earlier work (*Salpas* et al., 1986), we focus here on the geochemistry of micas exhibiting different pleochroic schemes.

Petrography

Several polished thin sections were prepared from the Blue Ball kimberlite samples and six were selected as best displaying the different phlogopite textures and types. Modes were calculated from approximately 2000 point counts of each thin section (Table 1); phlogopite makes up between 23 and 36 modal % of the Blue Ball kimberlite (Table 1). The kimberlite is comprised of phlogopite and serpentinized olivine phenocrysts (>1.5 mm) set in a groundmass of mica (<0.6 mm), chromite and titano-magnetite (<0.2 mm), rare perovskite (<0.2 mm), and carbonate ($\cong 0.1$ mm). The serpentinized olivine phenocrysts form the bulk of the kimberlite, comprising approximately 30–50 modal % (Table 1). These olivines have ragged and embayed margins, probably indicating resorption prior to serpentinization. Furthermore, the phlogopite phenocrysts also exhibit resorption textures, such as embayed grain boundaries and holes in the interiors of phenocrysts. Serpentinized olivine phenocrysts commonly have a corona of phlogopite (0.1–0.4 mm wide) that usually exhibits reverse pleochroism (Fig. 1D). These phenocrysts also contain small inclusions of phlogopite, which were probably formed at the time of alteration.

Table 1. *Modal analyses of six thin sections of the Blue Ball kimberlite.* Spinel represents both chromite and titano-magnetite

TS No.	OLIVINE	PHLOGOPITE	CARBONATE	SPINEL*	APATITE	PEROVSKITE
BB-1	36.3	32.8	20.7	10.1	---	0.1
BB-2	44.7	29.7	16.0	9.2	0.2	0.2
BB-3	46.3	23.0	20.6	10.1	---	---
BB-4	28.2	36.1	24.4	11.2	---	0.1
BB-5	52.0	23.5	12.4	12.1	---	---
BB-6	48.5	26.2	14.6	10.4	0.1	0.2

* = includes chromite and titano-magnetite. Chromite never exceeds 1%.

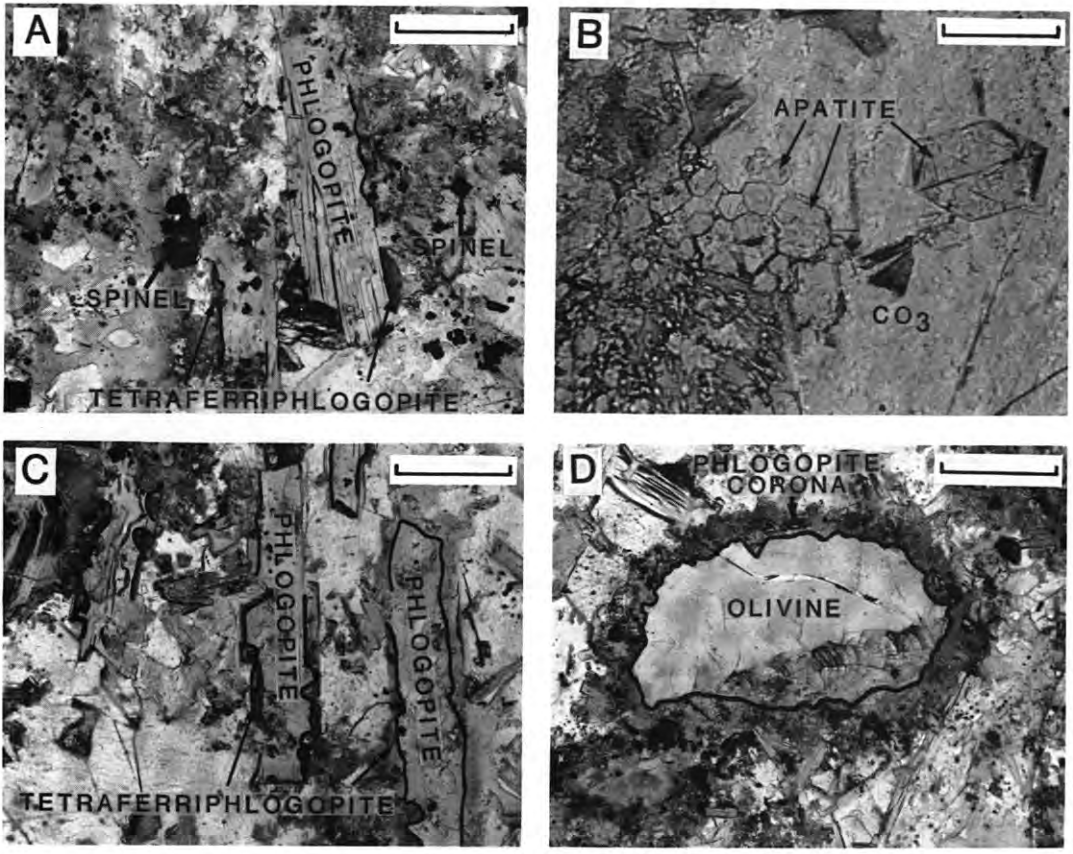

Fig. 1A. Photomicrograph of euhedral spinel inclusions in phlogopite phenocrysts with thin discontinuous tetraferriphlogopite rims (boundary enhanced). Scale bar = 0.25 mm
Fig. 1B. Photomicrograph of euhedral groundmass apatites with hexagonal morphology. Scale bar = 0.125 mm
Fig. 1C. Photomicrograph illustrating the nature of tetraferriphlogopite rims on phlogopite phenocrysts (boundary enhanced). Note the embayed core-rim contact of the phenocrysts. Scale bar = 0.25 mm
Fig. 1D. Serpentinized olivine phenocryst mantled by a phlogopite corona (boundary enhanced). Scale bar = 0.25 mm

Rarely, small inclusions of euhedral chromite ($\cong$0.05 mm) also are present in the serpentinized olivine phenocrysts.

The Blue Ball phlogopites do not display normal pleochroism [i.e., plane-polarized light (PPL) is most strongly absorbed parallel to the cleavage planes]. Rather, the common scheme is one of *reverse pleochroism* (PPL is most strongly absorbed perpendicular to the cleavage planes) or *intermediate pleochroism* (PPL most strongly absorbed between 0 and 90° to the cleavage planes). Phenocryst cores and most groundmass micas display intermediate pleochroism, whereas phenocryst rims exhibit reverse pleochroism (Fig. 1C). The phenocryst cores have embayed contacts with discontinuous rims of reverse pleochroism, indicating a replacement

texture (Fig. 1C). Similar textures are observed in some ($\cong 5\%$) groundmass phlogopites with cores of intermediate pleochroism. The rims of reverse pleochroism are usually thin (i.e., approximately 0.1–0.2 mm wide). Some groundmass micas exhibit total reverse pleochroism, indicative of complete replacement. We suggest that the groundmass grains of intermediate pleochroism, were originally phenocryst micas which have been severely resorbed by the residual magma. As such, they may only be distinguished from phenocryst cores on the basis of size.

The phlogopite phenocrysts are commonly truncated by olivine. These phlogopites contain occasional inclusions of chromite (Fig. 1A), indicative of early crystallization. All phlogopite laths are unoriented with only minor disruption of the cleavage planes (i.e., no kink bands; Figs. 1A and C), evidence that these micas were not crystallized before any violent magma movements. The phenocryst phlogopites form an interwoven network, the interstices of which are filled by groundmass phlogopites, carbonate ($\cong$12–25 modal %; Table 1), apatite ($\cong$0.1 mm and $\cong$ 0.2 modal %; Fig. 1B), perovskite ($<$0.05 mm and $\cong$0.1 modal %). Small (up to 0.2 mm), euhedral groundmass titano-magnetites ($\cong$8–9 modal %) are also abundant (*Salpas* et al., 1986).

Causes of Reverse Pleochroism in Micas

It was *Wones* (1963) and *Faye* and *Hogarth* (1969) who first attributed reverse pleochroism to the presence of tetrahedral Fe^{3+} in phlogopite. This type of pleochroism has been described in terms of Si and Al deficiency using the parameter $\Delta T = 8 - [Si + Al]$ (*Smith* et al., 1978), which describes tetrahedral site occupancy on the basis of 22 oxygens. *Farmer* and *Boettcher* (1981) suggested an alternative representation would be $\Delta T = 8 - [Si + Al + Ti]$. This observation was based on the fact that many of the micas with normal pleochroism which they studied had $Si + Al < 8$, but had $Si + Al + Ti > 8$. These authors suggested a sequence of tetrahedral site preference as $Si > Al > Ti > Fe^{3+}$. The parameters involved in the generation of different pleochroic schemes have the potential of providing a method for recognizing the physical and compositional nature of the magma(s) from which the phlogopites crystallized.

Work by *Seifert* and *Schreyer* (1971) and *Robert* (1976) suggested the possibility of Mg occupying the tetrahedral site in micas. The experimental results reported by these authors demonstrate that tetrahedral Mg only occurs in Al- and Fe-free micas. It is unlikely that these results can be applied to the Blue Ball phlogopites, as these contain both Al and Fe.

The rationale behind the choice of ΔT scheme to be used in this study of kimberlite micas requires some discussion. Contrary to the proposal of *Farmer* and *Boettcher* (1981), Ti is probably not a preferred occupant of the tetrahedral site (e.g., *Dawson* and *Smith*, 1977; *Dymek*, 1983; *S. Bailey*, 1984ab; *Guidotti*, 1984; *Rossman*, 1984). The preference of Fe^{3+} over Ti^{4+} in the tetrahedral site is also supported by considerations of ionic radii (*Whittaker* and *Muntus*, 1970). The ionic radius of Fe^{3+} (0.57 Å) is closer to Si^{4+} (0.34 Å) and Al^{3+} (0.47 Å) than Ti^{4+} (0.69 Å). Also, there is no direct evidence (i.e., absorption spectra) for tetrahedral Ti^{4+} such as exists for Fe^{3+} (e.g., *Faye* and *Hogarth*, 1969). Furthermore, the Blue Ball micas do not contain sufficient Ti to occupy tetrahedral site vacancies (see Table 2).

Mineral Chemistry

Mineral chemistry was determined using an automated CAMECA SX-50 electron microprobe at the University of Tennessee, Knoxville. Approximately 20–30 phlogopites were analyzed from each thin section. Normal operating conditions were 15 KV accelerating voltage and specimen current of ≅30 nA. Both natural and synthetic standards were used. The phlogopite analyses were corrected for matrix effects using standard ZAF procedures. Examples of the variation in phlogopite chemistry are presented in Table 2. Precision has been estimated, by duplicate analysis, to be ≅2% for oxides present in abundances >5 wt%, and 2–5% for oxides present in abundances <5 wt%.

Analyses of phlogopites exhibiting reverse pleochroism gave high cation totals (i.e., >16 on the basis of 22 oxygens). By allocating a large proportion of the Fe to

Table 2. *Representative phlogopite analyses from the Blue Ball kimberlite*

	CORE	RIM	CORE	RIM	CORE	RIM	CORONA	CORONA	GMASS	GMASS
SiO_2	39.4	40.3	40.1	40.7	38.7	37.4	43.1	41.6	38.8	39.7
TiO_2	1.47	0.69	0.82	0.45	1.14	1.24	0.24	0.14	1.79	1.10
Al_2O_3	12.4	2.12	12.7	1.25	11.6	4.75	0.09	0.07	7.02	11.1
Cr_2O_3	0.09	0.05	<0.03	0.18	0.22	0.23	0.12	0.11	0.29	0.46
FeO*	9.63	21.8	6.18	20.8	9.61	28.2	16.3	18.4	22.6	11.0
MnO	0.18	0.78	0.14	0.38	0.14	0.32	0.20	0.26	0.54	0.12
MgO	22.1	19.8	25.1	21.1	22.3	12.6	25.7	24.0	14.2	21.4
CaO	0.05	0.23	0.07	0.14	0.29	0.11	0.09	0.08	0.60	0.06
BaO	0.76	0.15	0.84	0.12	0.09	0.25	<0.10	<0.10	0.09	0.11
K_2O	10.3	10.2	10.4	9.96	10.5	9.75	9.76	9.49	9.60	10.3
TOTAL	**96.38**	**96.12**	**96.38**	**95.08**	**94.59**	**94.85**	**95.81**	**94.25**	**95.53**	**95.35**
	Formula moles based of 22 oxygens									
Si	5.729	6.298	5.745	6.383	5.740	6.116	6.521	6.485	5.898	5.852
Ti	0.158	0.078	0.084	0.050	0.126	0.148	0.026	0.014	0.195	0.121
Al	2.131	0.390	2.139	0.230	2.034	0.911	0.013	0.009	1.658	1.918
Cr	0.008	0.004	-----	0.018	0.026	0.028	0.013	0.009	0.051	0.052
Fe	1.170	2.847	0.739	2.720	1.193	3.847	2.061	2.396	2.870	1.360
Mn	0.021	0.101	0.017	0.046	0.017	0.043	0.022	0.032	0.093	0.013
Mg	4.784	4.616	5.354	4.929	4.921	3.070	5.802	5.575	3.219	4.717
Ca	0.004	0.037	0.008	0.023	0.017	0.048	0.013	0.009	0.093	0.008
Ba	0.042	0.004	0.046	0.004	0.013	0.004	-----	-----	0.004	0.004
K	1.918	2.021	1.899	1.993	1.986	2.029	1.883	1.884	1.901	1.932
TOTAL	**15.966**	**16.396**	**16.030**	**16.396**	**16.073**	**16.245**	**16.355**	**16.413**	**15.982**	**15.976**
MG#	80.3	61.9	87.9	64.4	80.5	44.4	73.8	69.9	52.9	77.6
ΔT	0.14	1.31	0.12	1.39	0.23	0.97	1.47	1.51	0.44	0.23

* = total Fe; GMASS = groundmass phlogopite; CORONA = phlogopite corona around serpentinized olivine phenocryst.

Table 3. *Compositional ranges exhibited by the different types of Blue Ball phlogopite*

	PHENOCRYST			
	CORE	RIM	GROUNDMASS	CORONA
SiO_2	36.8 - 40.5	35.7 - 40.9	36.8 - 40.4	39.7 - 43.1
TiO_2	0.77 - 2.25	0.05 - 3.93	0.43 - 3.74	0.04 - 0.55
Al_2O_3	7.87 - 13.3	0.17 - 7.36	3.57 - 12.3	0.07 - 1.40
Cr_2O_3	<0.02 - 0.34	0.04 - 0.23	<0.02 - 0.58	<0.02 - 0.12
FeO*	5.56 - 13.5	13.5 - 31.2	6.09 - 24.8	13.8 - 18.4
MnO	0.05 - 0.41	0.14 - 0.89	0.05 - 0.73	0.20 - 0.47
MgO	16.7 - 26.2	11.2 - 26.5	11.3 - 25.8	22.7 - 26.5
CaO	<0.02 - 0.41	0.27 - 2.48	<0.02 - 4.82	<0.02 - 1.11
BaO	0.26 - 1.40	<0.10 - 0.20	<0.10 - 0.61	<0.10 - 0.15
K_2O	6.30 - 10.5	6.70 - 10.3	7.52 - 10.9	9.11 - 10.6
MG#	76.2 - 89.1	39.0 - 74.7	45.4 - 88.3	69.2 - 76.6
ΔT	0.13 - 0.32	0.66 - 1.83	0.08 - 0.66	1.39 - 1.69

* = total Fe; GMASS = groundmass phlogopite; CORONA = phlogopite corona around serpentinized olivine phenocryst.

Fe_2O_3: 1) the formula mole total dropped to $\cong 16$, and 2) the analysis total came to a more reasonable value for phlogopite (minus H_2O). This indirect evidence supports our choice of ΔT scheme.

The phlogopite analyses have defined two phenocryst core compositions ("high" and "low" MG#), groundmass, phenocryst rim, and olivine corona compositions. Representative analyses of each occurrence of phlogopite are presented in Table 2, and ranges in composition of each of these is given in Table 3. Table 3 illustrates the wide range of MgO, FeO, and Al_2O_3 in the Blue Ball phlogopites. Generally, 25–35 phlogopite analyses were used to define each of the respective fields in the following Figures, except for the phlogopite coronas around serpentinized olivine phenocrysts (10) and the "high" MG# phenocryst cores (8). We have only plotted the "low" MG# phenocryst core compositions for which we have a rim analysis. Usually only one or two analyses were used to define an individual core and rim composition because of the zonation. For the coronas and groundmass compositions, 2–4 analyses defined these respective phlogopite compositions.

By comparison of Blue Ball phlogopite compositions (Tables 2 and 3) with those reported from other localities (e.g., *Dawson* and *Smith*, 1975; *Smith* et al., 1978; *Mitchell* and *Meyer*, 1980; *Farmer* and *Boettcher*, 1981; *Scott*, 1981; *Boctor* and *Boyd*, 1982; *Hunter* et al., 1984), it is evident that the Blue Ball micas exhibit a wide compositional range. For example, FeO extends up to 31 wt%, greater than any other reported kimberlite mica composition. Unlike the mica compositions reported by *Smith* et al. (1978), the Blue Ball phlogopites exhibit significant correlations with ΔT. However, there are no correlations between Cr_2O_3 and FeO or TiO_2, unlike those from Fayette County, Pennsylvania (*Hunter* et al., 1984). This is probably due to the relatively small ranges in Cr_2O_3 (<0.02–0.58 wt%) and TiO_2 (0.04–3.94 wt%) exhibited by Blue Ball phlogopites (Table 3). The remaining elements analyzed exhibit similar ranges as in other locations.

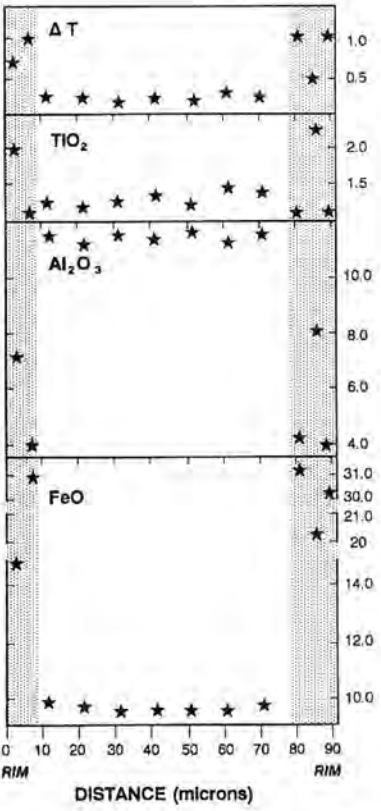

Fig. 2. An illustration of the chemical diversity across a phlogopite phenocryst from the Blue Ball kimberlite (after *Salpas* et al., 1986). Note that FeO and ΔT increases and Al_2O_3 decreases core-to-rim

An example of chemical variation across a Blue Ball phlogopite phenocryst is presented in Fig. 2. In terms of Al_2O_3, TiO_2, FeO, and ΔT, the core region is relatively homogeneous. The rim of reverse pleochroism displays a sharp increase in ΔT and FeO, and a decrease in Al_2O_3, relative to the core composition, with TiO_2 remaining *relatively constant* (supporting our choice of *Smith* et al.'s (1978) scheme for describing ΔT).

In order to use the phlogopite pleochroic schemes and mineral chemistry to trace the evolution of the kimberlite magma, we have plotted Magnesium number [MG# = molar (Mg/(Mg + Fe))*100], BaO, and TiO_2, each against ΔT.

MG# versus ΔT

The MG# for Blue Ball phlogopites varies from 39 to 89, with micas of intermediate pleochroism possessing the highest values. Groundmass micas generally have lower MG#'s (Fig. 3) than phenocryst cores, but many are similar. We conclude that those groundmass phlogopites with high MG#'s, were crystallized as phenocrysts which were subsequently resorbed, supporting the petrographic observations (see above). Therefore, in the following sections, the term groundmass refers to those phlogopites which may be separated from the phenocrysts on the basis of size **and** chemistry. Phenocryst rims are invariably similar to biotite (*Deer* et al., 1978), with MG#'s ranging from 39 to 78 (Table 1).

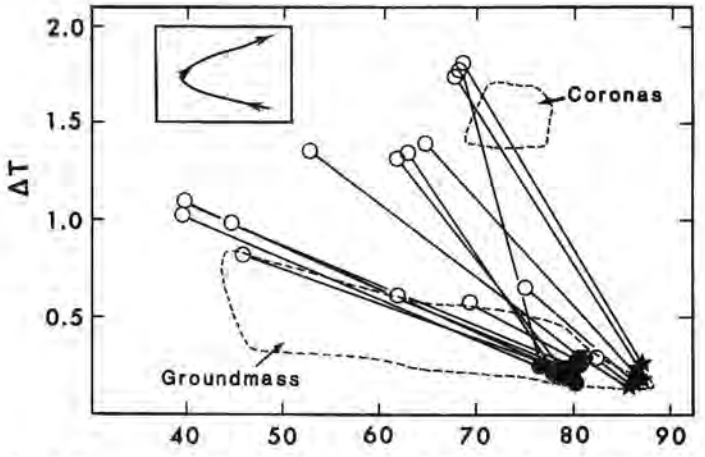

Fig. 3. Diagram of ΔT versus MG# for all Blue Ball phlogopites. Groundmass and corona phlogopites have been plotted as fields. Stars represent the earliest crystallized (highest MG#) group of phlogopite phenocrysts. Closed circles represent the second, later (lower MG#) group of phenocryst cores. Open circles represent phenocryst rims. Tie lines join core and rim analyses from the same phenocryst. The inset demonstrates the evolution path exhibited by Blue Ball phlogopites. The field of groundmass phlogopites is comprised of 35 analyses, and that of corona phlogopites is comprised of 10 analyses

Taken as a group, the groundmass phlogopites amd phenocryst cores from the Blue Ball kimberlite exhibit a decrease in MG#, following a *normal fractionation path* (Fig. 3). On the basis of MG#, there are two populations of phlogopite phenocryst cores: one of MG# 86–88 and one with MG# 76–81 (Fig. 3). Values of ΔT for these two groups overlap, but those with higher MG# generally have a lower ΔT. Two of the high MG# phenocrysts have rim compositions plotting in the lower MG# phenocryst group. The majority of the groundmass micas have ΔT values below 0.6 and have MG#'s which overlap with both populations of phenocryst cores extending to a MG# of 44.

The phenocryst rims and coronas around olivines exhibit an **increase** in MG#, depicting a *reversed fractionation trend* (Fig. 3), accompanied by higher ΔT values than the phenocryst cores and groundmass phlogopites. The phenocryst rims exhibit lower MG#'s than the corresponding cores and usually have a $\Delta T > 1$. The phlogopite coronas around the serpentinized olivine phenocrysts have high MG#'s ($\cong$71–79) and plot at the end of the trend defined by the phenocryst rims (Fig. 3).

TiO_2 versus ΔT

As demonstrated by Fig. 4, two groups of phenocryst cores are again present: a "low TiO_2" (0.77–0.95 wt%) and a "high TiO_2" (1.10–1.48) group. The latter has a slightly higher, although overlapping range in ΔT. Similar to Fig. 3, two phenocrysts have core compositions in the low TiO_2 phenocryst cores, and rim compositions plotting within the high TiO_2 group. Groundmass micas also overlap these groups and extend towards higher values of TiO_2 (up to 3.0 wt%) and ΔT (up to 0.6).

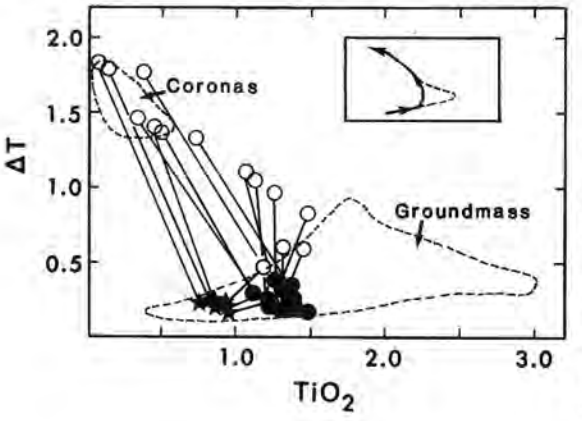

Fig. 4. Diagram of ΔT versus TiO_2 for all Blue Ball phlogopites. Symbols and inset as in Fig. 3. The tie lines represent a single phenocryst core and rim composition. The field of groundmass phlogopites is comprised of 35 analyses, and that of corona phlogopites is comprised of 10 analyses

A general trend of increasing ΔT with decreasing TiO_2 exists for the phenocryst rims. Phlogopite coronas around serpentinized olivine phenocrysts generally have the lowest TiO_2 abundances and the highest ΔT values.

BaO versus ΔT

The behaviour of BaO with ΔT (Fig. 5) is unlike that of either MG# or TiO_2. BaO exhibits a continual decrease with increasing ΔT. As seen in Fig. 3 and 4, there are two groups of phenocryst cores: a "high BaO" (0.75–0.95 wt%), and a "low BaO" (0.17–0.43 wt%) group. The second group has generally higher ΔT values. Two phenocrysts have core compositions in the high BaO group and rim compositions in the low BaO group. Groundmass phlogopites overlap these two groups, and some have no detectable BaO present (i.e., <0.03 wt%). In all cases, phenocryst rims contain less BaO than corresponding phenocryst cores. Phlogopites forming

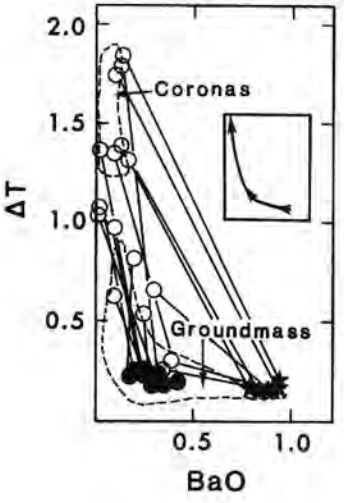

Fig. 5. Diagram of ΔT versus BaO for all Blue Ball phlogopites. Symbols and inset as in Fig. 3. The tie lines represent a single phenocryst core and rim composition. The field of groundmass phlogopites is comprised of 35 analyses, and that of corona phlogopites is comprised of 10 analyses

coronas around serpentinized olivine phenocrysts generally contain the least BaO, and the highest ΔT's.

CaO, Cr_2O_3, K_2O, SiO_2, and Al_2O_3

There is a general increase in both ΔT and CaO within the phenocryst cores and between core and rim (CaO can reach up to 2.8 wt% in the phenocryst rims). Corona phlogopites have practically no CaO (<0.1 wt%). The Cr_2O_3 contents are somewhat variable in abundance throughout the phlogopites. Generally, Cr_2O_3 increases from the phenocryst cores to the groundmass (up to 0.5 wt%) and then shows a marked decrease in the phenocryst rims. The K_2O contents exhibit little variation, ranging from 8.7 to 10.9 wt%, but the phenocryst rims and majority of groundmass phlogopites always contain less K_2O than the cores. Phlogopite coronas around serpentinized olivines have K_2O contents that practically span the range exhibited by the groundmass and phenocryst phlogopites.

Discussion

The compositional trends and pleochroic schemes within the Blue Ball phlogopites described above provide a unique insight into the crystallization of a kimberlite magma. The lack of megacryst phases in the Blue Ball kimberlite indicates that the evolution of the kimberlitic magma from generation to solidification is controlled totally by the observed mineral phases.

The formulated crystallization sequence uses the following assumptions: 1) olivine phenocrysts, phlogopite phenocryst cores, and minor chromite crystallized before the groundmass mica and titano-magnetite, and 2) the phenocryst cores with the highest MG# and lowest ΔT were the first to crystallize. As such, we have depicted evolution paths moving away from phlogopite phenocryst cores in the direction of magmatic evolution, on element-ΔT (see above) and element-element diagrams.

Significance of Reverse Pleochroism

The Blue Ball phlogopites contain insufficient Ti to fill the tetrahedral site, so the ΔT scheme proposed by Farmer and Boettcher is inappropriate here. We interpret the increase in ΔT (Figs. 3–5) to be the result of a gradual increase in the Fe^{3+} content of the residual magma. That Fe^{3+} increases is indirectly witnessed by increasing formula moles in phlogopites with reverse pleochroism (Table 1). If Fe^{3+} is calculated, the formula mole totals drop to near 16 (on the basis of 22 oxygens) for analyses of phlogopites which exhibit reverse pleochroism. Furthermore, there is an increase in Fe^{3+} from core to rim in the groundmass titano-magnetites (*Salpas* et al., 1986). This increase in Fe^{3+} can be explained if the fO_2 of the kimberlite magma decreased at a slower rate than that for normal buffer curves (e.g., the quartz-fayalite-magnetite buffer), such that fO_2 shows a relative increase, moving the magma towards higher Fe^{3+} concentrations.

All micas at Blue Ball have a positive ΔT, but not all exhibit reverse pleochroism. This suggests that reverse pleochroism requires a critical amount of tetrahedral Fe^{3+}, below which only intermediate pleochroism is present, or normal pleochroism persists. We conclude that intermediate pleochroism is a result of small amounts of

tetrahedral Fe^{3+} being present in the tetrahedral site (i.e., $\Delta T < 0.6$), and this type of pleochroism is distinctive of phenocryst cores and the majority of groundmass micas. The observed increase of Fe^{3+} in the residual magma produces the reverse pleochroism in later crystallized phlogopites (i.e., phenocryst rims, rare groundmass grains, and corona phlogopites). Note that these empirical chemical data remain to be substantiated by detailed absorption experiments.

Interpretation of Chemical Trends in Phlogopite

The basis for our interpretation of the chemical trends exhibited by the phlogopites is founded on the assumption that ΔT increases as crystallization proceeds (i.e., phlogopites with the lowest ΔT crystallized first). This may signify decreases in Si and Al in the kimberlite magma. However, although a decrease in Al is noted between core and rim in the phenocrysts, Si remains approximately constant or possibly exhibits an overall decrease followed by an increase (Fig. 6).

That phlogopite was a liquidus phase over practically the entire range of kimberlite crystallization is substantiated in Fig. 5. Phenocryst rims have decreased BaO concentrations relative to the phenocryst cores, as do the majority of groundmass micas. This is in response to phlogopite crystallization, as phlogopite is the only phase in the rock to incorporate Ba into its lattice. If there was a significant break in phlogopite fractionation, Ba would increase with ΔT in later phlogopites, which is not observed. Correlation of elements with ΔT allows the crystallization sequence and evolution of the Blue Ball kimberlite to be defined.

Petrographic observations indicate that early olivine fractionation occurred. This facilitated a decrease in MG#, and an increase in TiO_2 (Figs. 3 and 4) in the residual magma. As the parental magma is silica undersaturated, early combined olivine and phlogopite fractionation will tend to decrease Si in the residual magma (e.g., Fig. 6). Olivine fractionation continued during the crystallization of groundmass micas, as these also exhibit a progressive decrease in MG# with increasing ΔT (Fig. 3). TiO_2 increases in the residual melt as long as MG# decreases.

The rims of the phlogopite phenocrysts exhibit an increase of MG# with increasing ΔT (Fig. 3), leading to the majority of phlogopite coronas around olivine phenocrysts containing high MG#'s, but also with high ΔT's (Fig. 3). We consider these phlogopite coronas to be the last micas to crystallize as they contain amongst

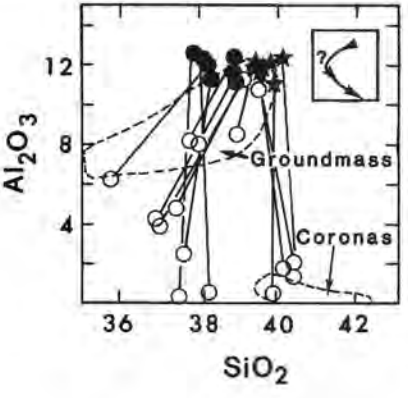

Fig. 6. Diagram of Al_2O_3 versus SiO_2 for all Blue Ball phlogopites. Symbols and inset as in Fig. 3. The tie lines represent a single phenocryst core and rim composition. The field of groundmass phlogopite is comprised of 35 analyses, and that of corona phlogopites is comprised of 10 analyses

the highest ΔT values (Figs. 3–5). Furthermore, these particular phlogopites exhibit a decrease in TiO_2 (Fig. 4). We attribute this to the removal of olivine from the liquidus and the major fractionation of groundmass titano-magnetite. The increase in MG # during magma evolution (i.e., the reverse of what is normally expected) is somewhat surprizing, but in no way unique. *Brooks* and *Rucklidge* (1973) and *Weiblen* et al. (1981) report a core-to-rim increase in MG # in clinopyroxene phenocrysts from alkali basalts. These authors suggest that oxidation of Fe^{2+} to Fe^{3+} (by a relative increase in fO_2) has facilitated this reversed compositional trend, and supports our contention of increased Fe^{3+} producing reversed pleochroism in late-stage phlogopites. Such a scenario during the crystallization of the Blue Ball kimberlite could have produced the increase in MG # observed in the phlogopite phenocryst rims. The evidence presented above for an increase in Fe^{3+} in the residual magma supports the idea of a relative increase in fO_2 during the later stages of crystallization.

Minor chromite is present as early-formed inclusions in both phlogopite and olivine phenocrysts. These show similar, though less pronounced, zonation as in groundmass titano-magnetites (*Salpas* et al., 1986). The Fe and Ti concentrations in these minor chromite inclusions will not facilitate a decrease of these elements in the residual liquid. This is because the TiO_2 (and Cr_2O_3) increase in the residual magma produced by major olivine fractionation is not reversed by this relatively minor chromite precipitation. The effects of olivine and titano-magnetite crystallization on the residual magma is exemplified in Fig. 7. Here, FeO is plotted against

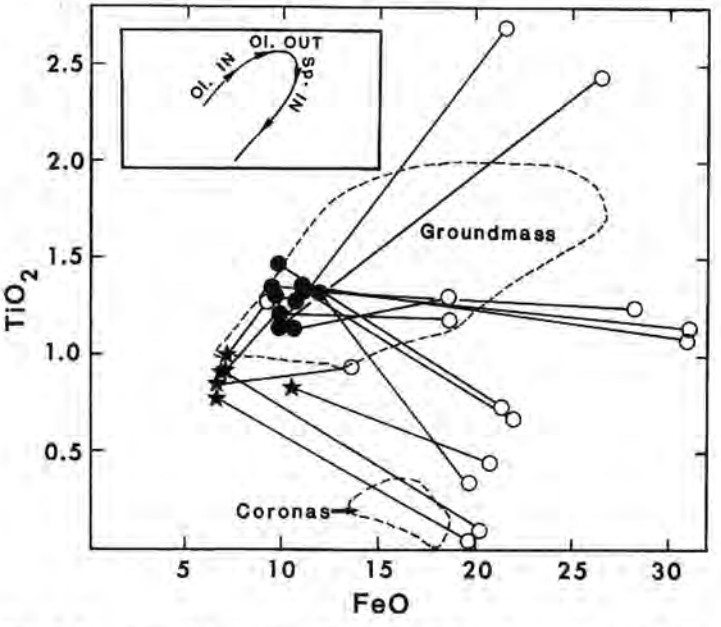

Fig. 7. Diagram of FeO versus TiO_2 for all Blue Ball phlogopites. Symbols and inset as in Fig. 3. The tie lines represent a single phenocryst core and rim composition. The field of groundmass phlogopites is comprised of 35 analyses, and that of corona phlogopites is comprised of 10 analyses

TiO_2 in the phlogopites. The removal of olivine from the liquidus and increased fractionation of titano-magnetite produces a decrease in Fe and Ti and a decrease of MG # in both phenocryst rims and corona phlogopites.

Crystallization and Origin of the Blue Ball Kimberlite

Due to the lack of suitable mineral assemblages required for geothermobarometric calculations, the depth of origin of the phlogopite and olivine phenocrysts cannot be directly estimated. The maximum depth of derivation can be placed at the limit of phlogopite stability, at about 150–200 km (e.g., *Eggler* and *Wendlandt*, 1978; *Wendlandt* and *Eggler*, 1980).

We present our preferred interpretation of the paragenetic sequence for kimberlite crystallization in Fig. 8. The phlogopite phenocrysts were derived from the kimberlite magma and give no indication of a xenocrystal origin (*Salpas* et al., 1986). The petrography and high MG # of these phlogopite phenocrysts indicate that they represent an early period of crystallization, probably at depth. The presence of two phenocryst core populations suggest an interruption of phlogopite crystallization. The decrease in MG # between the two populations suggests olivine also was an early, but uninterrupted liquidus phase (Fig. 8). The idea that these two populations may be a statistical artifact is unfounded. Two phenocryst cores, high in MG #, BaO, and low in TiO_2 have rim compositions identical to the second group of phenocryst cores that are low in MG #, BaO, and high in TiO_2. More high MG #

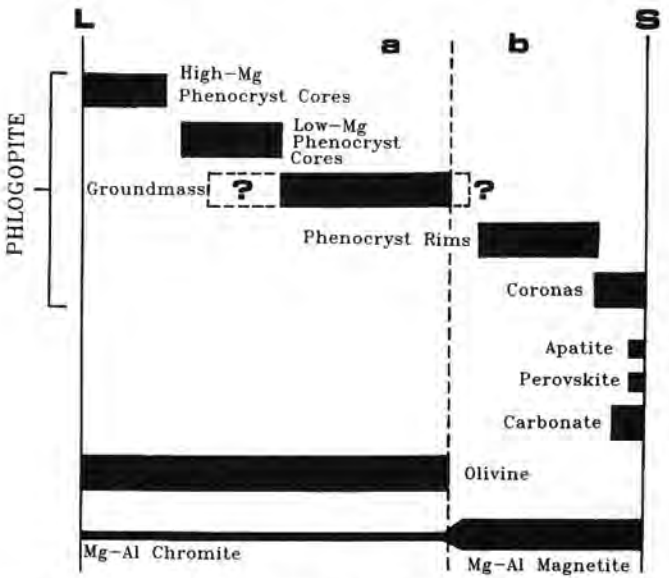

Fig. 8. Schematic diagram of the Blue Ball kimberlite paragenetic sequence. The dashed outline on part of the groundmass field indicates uncertainty as to whether phlogopite of this type crystallized at this time. There is a relative fO_2 increase from field A to field B and it is in field B that the tetraferriphlogopites (i.e., those exhibiting reverse pleochroism) crystallized. *L* liquidus; *S* solidus

phlogopite phenocryst cores containing rims of similar composition to the second phlogopite phenocryst cores are probably present, but have not been sampled in this study. Therefore, crystallization of the second phlogopite phenocryst group also formed as overgrowths on earlier surviving mica phenocrysts. After this second phenocryst crystallization event, the majority of the groundmass micas were precipitated (Fig. 8). There is a continuous compositional range from the phenocryst cores to the groundmass, with an increase in ΔT (0.08–0.6).

After olivine and early phlogopite crystallization, the residual kimberlite magma and phenocrysts were emplaced into the crust, where olivine fractionation was effectively halted (Fig. 8). In doing so, the kimberlite magma entered a lower pressure regime without initially adjusting to ambient temperatures. Considering the negative dP/dT of the kimberlite solidus (e.g., *Eggler* and *Wendlandt*, 1979), this movement imparted a significant amount of superheat to the magma, creating holes and ragged margins in the phlogopite phenocrysts by partial resorption. A passive emplacement is inferred in order to account for the lack of xenoliths at this locality and the undeformed nature of phlogopite cleavage planes.

A third period of phlogopite crystallization was initiated as the magma temperature adjusted to crustal conditions. Phlogopites that crystallized during this period continued to grow on previously crystallized phases, explaining the lack of discrete phlogopites with these compositions. This third stage of mica crystallization is represented by an **increase** in MG# and **decrease** in TiO_2 with increasing ΔT. MG# increases due to the widespread fraction of titano-magnetite and cessation of olivine crystallization (Fig. 8). Furthermore, phlogopites that crystallized during this time exhibit reverse pleochroism, suggesting that Fe^{3+} increased in the residual magma (indicating a relative increase in fO_2) as kimberlite crystallization proceeded. The majority of phlogopite coronas around olivine phenocrysts were the last to form as they have relatively high MG#'s and amongst the highest ΔT values. There was a relative increase in fO_2 throughout this fractionation sequence, as witnessed by the eventual crystallization of tetraferriphlogopites.

The general increase in Ca from phenocryst cores to the rims indicates the lack of a high-Ca phase on the liquidus (i.e., clinopyroxene) during kimberlite crystallization. Although rare perovskite and apatite occur in the groundmass, these are probably the final phases to crystallize from the Ca enriched residual magma (Fig. 8).

Summary

The lack of megacrysts indicates that the mineral phases present have controlled the chemical evolution of the Blue Ball kimberlite during its crystallization. The mineralogical evolution appears to have been accompanied by a relative increase in fO_2, witnessed by an increase in Fe^{3+} in spinels (*Salpas* et al., 1986) and high cation totals in phlogopite rims, attributable to the presence of Fe^{3+}. The increase in Fe^{3+} is also considered to produce the reverse pleochroism observed in later crystallized phlogopites. The reversal of pleochroism is produced by Fe^{3+} being present in the tetrahedral site of the phlogopite.

As phlogopite has crystallized over practically the whole range of solidification, the variations in chemistry of the residual magma will be reflected in this mineral phase. We conclude that the following sequence of kimberlite crystallization for the

Blue Ball kimberlite can satisfactorily explain the phlogopite mineral chemistry (Fig. 8):

1. Olivine, minor chromite, and Mg-rich phlogopite phenocrysts;
2. Olivine and minor chromite only during a halt in phlogopite crystallization and resorption of earlier micas;
3. Olivine, minor chromite, and phlogopite phenocrysts of lower MG# and groundmass micas;
4. Titano-magnetite and phlogopite exhibiting reverse pleochroism;
5. Perovskite and apatite crystallization, possibly with phlogopite coronas on olivine phenocrysts.

Olivine was no longer fractionated after the magma was emplaced into the crust and deuteric alteration (serpentinization) occurred at this time. Minor oxide (chromite) crystallization occurred during stages 1–3, but this did not affect the chemistry of the residual magma to an extent which could deduced from phlogopite compositions.

The Blue Ball kimberlite affords a unique opportunity to track its chemical evolution and emplacement into the crust. It behooves us to consider the possibility of such a study on similar occurrences worldwide, in order to deduce whether this crystallization model is applicable to other micaceous kimberlites.

Acknowledgments

This paper has benefitted from discussions with, and the constructive criticisms of Drs. *S. E. Haggerty, T. C. Labatka, A. L. Montana, J. J. Papike, P. A. Salpas,* and *J. W. Shervais.* Thoughtful reviews from *P. W. Weiblen* and two anonymous reviewers have enhanced the quality of this manuscript. *P. A. Salpas* is thanked for stimulating this study of the Blue Ball kimberlite. The Cameca electron microprobe was purchased with grants provided by NASA and NSF to L.A.T. A portion of this research was also supported by NASA grant NAG 9–73 to L.A.T.

References

Bailey DK (1982) Mantle metasomatism—continuing chemical change within the Earth. Nature 296: 525–530

— (1984) Kimberlite: The mantle sample formed by ultra-metasomatism. In: *Kornprobst J* (ed) Kimberlites I: Kimberlites and related rocks, pp 323–333

Bailey SW (1984a) Classification of micas. In: *Bailey SW* (ed) Reviews in mineralogy, 13: Micas. Mineralogical Society of America, Washington, DC, pp 1–12

— (1984b) Crystal chemistry of the true micas. In: *Bailey SW* (ed) Reviews in mineralogy, 13: Micas. Mineralogical Society of America, Washington, DC, pp 13–60

Boctor NZ, Boyd FR (1982) Petrology of the kimberlite from the De Bruyn and Martin Mine, Bellsbank, South Africa. Amer Mineral 67: 917–925

Boettcher AL, O'Neil JR, Windom JE, Stewart DC, Wilshire HG (1979) Metasomatism of the upper mantle genesis of kimberlite and other volcanics. In: *Boyd FR, Meyer HOA* (eds) Kimberlites, Diatremes, and Diamonds. AGU Washington, pp 173–182

Brooks CK, Rucklidge JC (1973) A Tertiary lamprophyric dike with high-pressure xenoliths and megacrysts from Wiedemanns Fjord, East Greenland. Contrib Mineral Petrol 42: 197–212

Dawson JB, Smith JV (1975) Chemistry and origin of phlogopite megacrysts in kimberlite. Nature 253: 336–338

— — (1977) The MARID (mica-amphibole-rutile-ilmenite-diopside) suite of xenoliths in kimberlite. Geochim Cosmochim Acta 41: 309–323

Deer WA, Howie RA, Zussman J (1978) An introduction to the rock forming minerals. Longman, London, 528pp

Delaney JS, Smith JV, Carswell DA, Dawson JB (1980) Chemistry of micas from kimberlites and xenoliths—II. Primary- and secondary-textured micas from peridotite xenoliths. Geochim Cosmochim Acta 44: 857–872

Dymek RF (1983) Titanium, aluminum, and interlayer cation substitutions in biotite from high grade gneisses, West Greenland. Amer Mineral, 68: 880–899

Eggler DH, Wendlandt RF (1978) Phase relations of a kimberlite composition. Carnegie Institute of Washington Yearbook 77: 751–756

— — (1979) Experimental studies on the relationship between kimberlite magmas and partial melting of peridotite. In: *Boyd FR, Meyer HOA* (eds) Kimberlites, diatremes, and diamonds: Their geology, petrology, and geochemistry. American Geophysical Union, Washington, pp 330–338

Erlank AJ, Allsopp HL, Hawkesworth CJ, Menzies MA (1982) Chemical and isotopic characterization of upper mantle metasomatism in peridotite nodules from the Bultfontein kimberlite. Terra Cognita 2: 261–263

Farmer GL, Boettcher AL (1981) Petrologic and crystal-chemical significance of some deep-seated phlogopites. Amer Mineral 66: 1154–1163

Faye GH, Hogarth DD (1969) On the origin of "reverse pleochroism" of a phlogopite. Can Mineral 10: 25–34

Guidotti CV (1984) Micas in metamorphic rocks. In: *Bailey SW* (ed) Reviews in mineralogy, 13: Micas. Mineralogical Society of America, Washington, DC, pp 357–467

Hunter RH, Kissling RD, Taylor LA (1984) Mid- to late-stage kimberlitic melt evolution: Phlogopites and oxides from the Fayette County kimberlite, Pennsylvania. Amer Mineral 69: 30–40

Jones RA (1984) Geochemical and isotopic studies of some kimberlites and included ultrabasic xenoliths from southern Africa. Unpublished PhD thesis, University of Leeds, UK

Kushiro I (1975) On the nature of silicate melt structure and its significance in magma genesis: regularities in the shift of the liquidus boundaries involving olivine, pyroxene, and silica minerals. Amer J Sci 275: 411–431

Lloyd FE, Bailey DK (1975) Light element metasomatism of the continental mantle: the evidence and the consequences. Phys Chem Earth 9: 389–416

Menzies MA, Hawkesworth CJ (1987) Mantle metasomatism. Academic Press, New York, 472pp

Mitchell RH, Meyer HOA (1980) Mineralogy of micaceous kimberlite from the Jos dike, Somerset Island. Can Mineral 18: 241–250

Robert J-L (1976) Phlogopite solid solution in the system K_2O–MgO–Al_2O_3–SiO_2–H_2O. Chem Geol 17: 195–212

Rossman GR (1984) Spectroscopy of micas. In: *Bailey SW* (ed) Reviews in mineralogy 13: Micas, Mineralogical Society of America, Washington, DC, pp 145–181

Salpas PA, Taylor LA, Shervais JW (1986) The Blue Ball kimberlite. J Geol 94: 891–901

Scott BH (1981) Kimberlite and lamproite dikes from Holsteinberg, West Greenland. Medd Gronland Geoscience 4: 3–24

Seifert F, Shreyer W (1971) Synthesis and stability of micas in the system K_2O–MgO–SiO_2–H_2O and their relationships to phlogopite. Contrib Mineral Petrol 30: 196–215

Smith JV, Brennesholtz R, Dawson JB (1978) Chemistry of micas from kimberlites and xenoliths—I. Micaceous kimberlites. Geochim Cosmochim Acta 42: 959–971

Wass SY, Rogers NW (1980) Mantle metasomatism—precursor to continental alkaline volcanism. Geochim Cosmochim Acta 44: 1811–1823

Weiblen PW, Stuckless JS, Hunter WC, Schulz KJ, Mudrey MG, Jr (1981) Correlation of clinopyroxene compositions with environment of formation based on data from Ross Island volcanic rocks. In: Dry Valley Drilling Project, Antarctic Research Series 33: 229–246

Wendlandt RF, Eggler DH (1980) The origin of potassic magmas: 2. Stability of phlogopite in natural spinel lherzolite and in the system $KAlSiO_4$–SiO_2–H_2O–CO_2 at high pressures and high temperatures. Amer J Sci 280: 421–437

Whittaker EJW, Muntus R (1970) Ionic radii for use in geochemistry. Geochim Cosmochim Acta 34: 945–956

Wones DR (1963) Phase equilibria of "Ferriannite", $KFe_3^{2+}Fe^{3+}Si_3O_{10}(OH)_2$. Amer J Sci 261: 581–596

Wyllie PJ (1978) Mantle fluid compositions buffered in peridotite–CO_2–H_2O by carbonates, amphibole, and phlogopite. J Geol 86: 687–713

— (1979) Kimberlite magmas from the system peridotite–CO_2–H_2O. In: *Boyd FR, Meyer HOA* (eds) Kimberlites, Diatremes, and Diamonds, AGU Washington, pp 319–329

Authors' address: Dr. *Clive R. Neal* and *L. A. Taylor*, Department of Geological Sciences, University of Tennessee, Knoxville, TN 37996, U.S.A.

Printed in Austria